RSC Advances

PAPER

Cite this: *RSC Adv.*, 2021, **11**, 28029

Green synthesis of gold nanoparticles using an antiepileptic plant extract: *in vitro* biological and photo-catalytic activities†

Jayanta S. Boruah,‡[ab] Chayanika Devi,‡[c] Upasana Hazarika,[d] P. Vijaya Bhaskar Reddy,[c] Devasish Chowdhury,*[a] Manash Barthakur[e] and Pankaj Kalita*[f]

Gold nanoparticles are one of the widely used metallic nanoparticle having unique surface plasmon characteristic, offers major utility in biomedical and therapeutic fields. However, chemically synthesized nanoparticle creates toxicity in the living organisms and contradicts the eco-friendly and cost-effective nature. So, developing greener synthetic route for synthesis of gold nanoparticle using natural materials is an enthralling field of research for its effectiveness in synthesizing eco-friendly, non-toxic materials. Moreover, biological components attached as stabilizing agent can exert its own effect along with the advantages of nanoparticle conjugation. In this work, we used for the first time methanolic leaf extract of *Moringa oleifera* as this fraction of *M. oleifera* exerts a neuroactive modulation against seizure as evidenced by earlier literature. The green gold nanoparticles synthesized were characterized by different characterization tools, dynamic light scattering and transmission electron microscopy techniques *etc.* Prepared nanoparticles were biologically (antioxidant, antimicrobial and blood cytotoxicity) characterized to screen their further utility in therapeutic strategies. Characteristics and activities of green gold nanoparticles were compared with conventional citrate stabilized gold nanoparticles. It was observed that green gold nanoparticles prepared using *M. oleifera* show less cytotoxicity and helps in regeneration of neuronal cells in animal model study. It establishes the fact that conjugation of different plant extract fraction for stabilization of gold nanoparticle may be responsible factor for enhancement of bioactive nature of green gold nanoparticle. In addition, the green gold nanoparticle show efficient photo-catalytic efficiency. Development of such bioactive gold nanoparticles will lead to functional materials for biomedical and therapeutic applications.

Received 5th April 2021
Accepted 28th July 2021

DOI: 10.1039/d1ra02669k

rsc.li/rsc-advances

1 Introduction

The nanoparticle plays a fascinating role in modern biological science researches, mainly in the field of catalysis,[1] sensory probes[2–4] as well as in diverse field of medical science such as therapeutic agents, drug delivery,[5,6] very recently in toxin removal[7] *etc.* Nanoparticles show higher level of performance in compared to its parent bulk material because of its high surface to volume ratio, size, shape and charge characteristics along with its high reactivity.[8] Metallic nanoparticles, like gold nanoparticle (AuNP), with integration of tailored functional properties, present a valuable precursor for rational design of innovative nanodevices and nanosystems.[9] The optical characteristic offered by the characteristic Surface Plasmon Resonance (SPR) of AuNP leads to its multiple usability in bioscience and biomedical applications, like bioinstrumentation, disease diagnosis, drug delivery, gene therapy, as biosensor *etc.*[9–11] Although, there are several standardized methods of gold nanoparticle synthesis using different stabilizing agents but chemically synthesized nanoparticle have some drawbacks like biological toxicity, ecological imbalance and moreover, the cost involving in its synthesis. Moreover, in such procedures, traces of unreacted reagents or unwanted by-products remain in the gold colloidal solution interpreting the chemically synthesized AuNPs unsuitable and problematic for its further biological applications.[12] In recent years, green chemistry pathway by utilizing plant extract for the biosynthesis of AuNPs has gained importance over chemical routes of AuNP synthesis due to its simplicity for rapid synthesis during reduction of their parent.[13]

[a]*Material Nanochemistry Laboratory, Physical Sciences Division, Institute of Advanced Study in Science and Technology, Paschim Boragaon, Garchuk, Guwahati, 781035, India. E-mail: devasish@iasst.gov.in*

[b]*Department of Chemistry, Cotton University, Assam, India*

[c]*Department of Life Science and Bioinformatics, Assam University, Diphu Campus, Diphu, Assam, India*

[d]*Department of Biophysics, Pub Kamrup College, Baihata Chariali, Assam, India*

[e]*Department of Zoology, Pub Kamrup College, Baihata Chariali, Assam, India*

[f]*Department of Zoology, Eastern Karbi Anglong College, Karbi Anglong, Assam, India. E-mail: kalita.pankaj9@gmail.com*

† Electronic supplementary information (ESI) available. See DOI: 10.1039/d1ra02669k

‡ Both the authors have equal contribution.

Its suitability appears in terms of its cost effectiveness and eco-friendly nature. In addition, it is reported that such green synthesized nanoparticles are safe for clinical research over chemically synthesized nanoparticle.[14] In this line, use of medicinal plant extract (like having antioxidant behaviour) has been demonstrated for gold nanoparticle synthesis by various groups earlier.[15] Similarly, fruits waste materials (banana peels) with high medicinal value are also applied to prepare gold nanoparticles.[16]

It is interesting to note that a well-known plant "*Moringa oleifera*" has been playing a remarkable role in the pharmacology of human health in terms of nutrition and medicine.[17] It has been proved to be contained a variety of bioactive compounds of pharmacological importance.[18] Different *in vitro* and *in vivo* studies have already confirmed the pharmacological significance of *M. oleifera* leaves.[18] Presence of different bioactive molecules might be the supporting reason for its wide use as medicinal source for various ailments. The *M. oleifera* leaves are well-known source of pharmaceutical value for different infectious diseases like malaria and typhoid fever and hypertension and diabetes.[19] Recently, aqueous extract of this particular plant leaves has been used for synthesis of gold nanoparticles and some important biological assays were evaluated.[20] However, it is interesting to note that the methanolic extract of leaves of *M. oleifera* has neuroactive properties specially the antiepileptic nature.[21–23] It has not been applied in nanoparticles synthesis so far. Therefore, in the present investigation, methanolic leaf extract of a traditional medicinal plant *Moringa oleifera* (family: Moringaceae, commonly known as drumstick)[24] was used for the synthesis of AuNP. The leaf of the plant was used depending on their maturity ages for extract preparation and AuNP synthesis was performed depending on different physical parameters like temperature, pH *etc.* Further, the characteristics and stability of differently prepared AuNPs were analysed. Synthesized AuNPs were employed for different biomedical applications like antioxidant properties and antimicrobial activities as well as photo-catalytic activity. Further, it was studied to reveal the cytotoxicity of the green AuNPs on blood cells as it is the first line of exposure that comes in contact when administered to body as drug molecule or bioactive supplements. Effect of *M. oleifera* stabilized AuNP was further authenticated by seeing its effect on brain architecture. This report will be a first of its kind although silver nanoparticles have been synthesized using the leaf extract of *M. oleifera*.[25] The whole synthesis protocol is represented as shown in Scheme 1.

2 Experimental

2.1 Materials and method

Tri-sodium citrate dihydrate, ascorbic acid, methylene blue and methanol were purchased from Merck, India. Gold chloride salt ($HAuCl_4 \cdot 3H_2O$) and 2, 2-diphenyl-1-picrylhydrazyl (DPPH) were bought from Sigma Aldrich. Muller-Hinton media and standard antibiotics procured from Himedia, India. The all chemicals and reagents used in the entire study were of analytical grade. Distilled water was used throughout the experiment. All the chemicals were used without further purification.

2.2 Preparation of methanolic extract of *Moringa oleifera*

Fresh immature, mature and old aged leaves of healthy *Moringa oleifera* plants were collected from the local area of Baihata chariali of Assam, India and cleaned with tap water and finally rinsed with distilled water. The leaves were air dried at shade environment at room temperature and were finely powdered. 30 g of each powdered plant material was dissolved in 250 mL methanol. The mixture was extracted in the Soxhlet apparatus for 10 h at 35–45 °C. The extracts were concentrated using rotary vacuum evaporator at 45 °C under low pressure. The extracts were filtered and the solvent was evaporated and the extract was concentrated using vacuum rotary evaporator. The extracted solution was homogenized by stirring and then centrifuged for 2 minutes, followed by filtering through a 0.45 μm filter. All the extracts were kept frozen at 8 °C until used.[21–23]

2.3 Preparation of gold nanoparticles – chemical and green approach

Chemically, gold nanoparticle was prepared using gold chloride ($HAuCl_4 \cdot 3H_2O$) as the parent chemical and tri-sodium citrate was used as the stabilizing agent. A reaction volume of 20 mL of strength 394 μg mL^{-1} $HAuCl_4 \cdot 3H_2O$ was stirred continuously at 850 rpm at a temperature of 60 °C for 20 minutes and

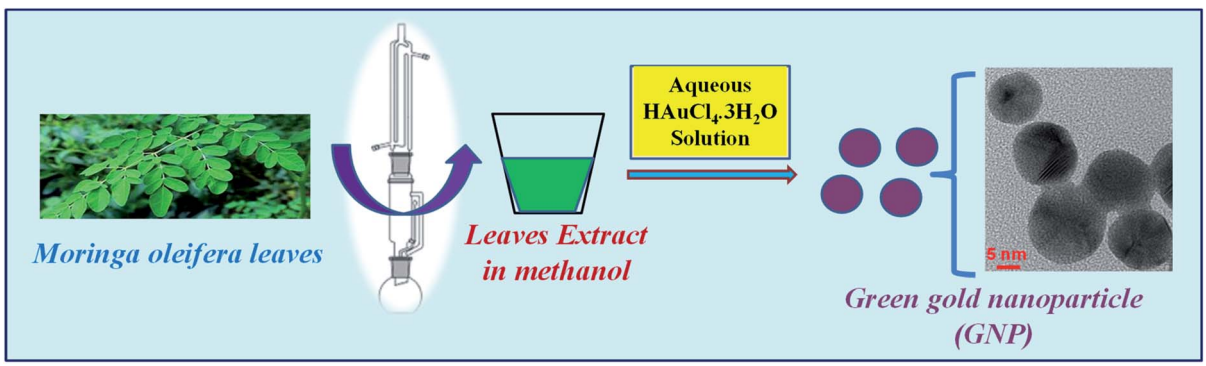

Scheme 1 A pictorial representation of the preparation of *M. oleifera* leaves extract in methanol followed by synthesis of green gold nanoparticles, reduced and stabilized by methanolic extract of *M. oleifera* leaves.

immediately 4 mL of 10^5 μg mL^{-1} solution of tri-sodium citrate was added. The change in color of gold chloride solution indicates the formation of gold nanoparticles. The final nanoparticles dispersion (328 μg mL^{-1} with respect to $HAuCl_4$) was filtered with 0.22 μm syringe filter and the citrate stabilized gold nanoparticles (denoted as gnp-citrate) were stored in 4 °C for further use.[26]

Biosynthesis of gold nanoparticle was carried out using the same parent compound $HAuCl_4 \cdot 3H_2O$. Instead of tri-sodium citrate as the stabilizing agent, in biosynthesis process, methanolic leaf extract of *M. oleifera* was used as the stabilizing agent. Typically, 4 mL of the *M. oliefera* leaf extract (10^5 μg mL^{-1} in 2% DMSO in water) was added to the 20 mL gold chloride solution (394 μg mL^{-1} concentration) with similar condition. The mixture was kept under continuous stirring on a magnetic stirrer at temperature of 75 °C till the color of the mixture becomes reddish brown indicating the reduction of Au^{3+} to Au^0 in NPs which is dependent on several parameters, such as the extract concentration, the temperature and pH of the reaction solution.[27] UV-Vis spectrum was observed for confirmation of the gold nanoparticle formation using UV-Vis spectrophotometer.[28] The prepared green gold nanoparticle (denoted as GNP) mixture was filtered with 0.22 μm syringe filter and centrifuged at 5000 rpm for 30 min to settle down the unwanted heavy materials.[29] The final concentration of the so formed gold nanoparticles dispersion is 328 μg mL^{-1} with respect to $HAuCl_4$ used.

2.4 Characterization

The methanolic leaves extract was subjected to different spectroscopic tools like FTIR, UV-Vis spectroscopies to get the chemical and optical properties along with qualitative phytochemical analysis to detect the presence of various biomolecules. The complete methods of phytochemical analysis have been incorporated in the ESI.† Further, different spectroscopic techniques were used to characterize the prepared nanoparticles. UV-Vis spectra were collected on a UV-Vis spectrophotometer (Eppendorf, Biospectrometer basic). Particle size and zeta potential measurement were performed on a Malvern Zetasizer Nano series, Nano-ZS90. Transmission electron microscope (TEM-2100 Plus, JEOL) was used to get particle structure and morphology. Fourier Transform Infrared Spectra (FTIR) was collected on a Nicolet-6700 FTIR spectrophotometer to find out the functional groups. Fluorescence spectra were recorded using Jasco spectrofluorometer FP-8300. X-ray diffraction (XRD) pattern was observed at a Rigaku smartLab XRD set up.

2.5 Determination of band gap energy using UV-Vis spectrum and stability of citrate stabilized and green gold nanoparticles

The both nanoparticles, vizually citrate stabilized and green gold nanoparticles (synthesized with immature, mature and old leaves) were analyzed to get UV-Vis spectra in water medium at particular time interval ($t = 0$, 15 and 30 days).

The direct band gap of as prepared samples can be estimated from the graph of $h\nu$ *versus* $(\alpha h\nu)^2$ which is well known as Tauc plot for the absorption coefficient α which is related to the band gap E_g as $(\alpha h\nu)^2 = k(h\nu - E_g)$, where $h\nu$ is the incident light energy and k is a constant. The relationship is also known as Tauc equation which is useful for determination of band gap, E_g. The linear region in the Tauc plot will give a tangent near the point of maximum slope. The extrapolation of the tangent or straight line in Tauc plot to $(\alpha h\nu)^2 = 0$, gives the value of band gap energy E_g.[30] From the UV-Vis spectra and corresponding band gap for each sample throughout the time, stability can be explained.[31]

Also, effect of pH on the stability of green gold nanoparticles was evaluated at three different pH (3.4, 6 and 9.6). Here, our optimized reaction condition was maintained and pH was varied to get subsequent data.

2.6 Cytotoxicity of AuNP by haemolytic potentiality test in blood cells

An *in vitro* hemolytic potentiality test was performed in accordance with protocol reported by Mishra *et al.* (2013), with slight modification.[32] Briefly, blood samples were collected from the medical laboratory technician course laboratory of Pub Kamrup College, Assam, India from five healthy human subjects. The blood sample was centrifuged at 900 rpm for 12 min with three repeated washing using 0.9% saline solution. The settled RBC was suspended in phosphate buffer saline (pH 7.4) and kept in a special buffer composed of a standard amount of protein dissolved in normal saline mimicking the body fluid composition. The suspended RBC treated with various concentrations (0.25 to 5.0 μL mL^{-1}) of AuNPs stock solution (dispersed in PBS buffer). As a negative control, the SDS (1%) was used which is capable of rupturing the red blood cells and PBS is used as positive control. For the assay, 200 μL of the dissolved samples and 800 μL of RBC were added and incubated at 37 °C for 90 min. After incubation, the samples were centrifuged at 2000 rpm for 10 min and the supernatant was carefully transferred for determining the percentage of hemolysis at absorbance of 540 nm in UV-Vis spectrophotometer. The percentage of hemolysis was calculated as follows:

$$\text{Percentage of hemolysis } (\%) = \frac{X - Y}{Z - Y} \times 100$$

where, X= absorbance of nanoparticle treated RBC; Y = absorbance of PBS treated RBC; Z= absorbance of SDS treated RBC.

2.7 Microscopic observation of AuNP treated blood cells

The precipitated erythrocytes (after centrifugation of treated sample) were stained with Leishman stain using standard protocol for further microscopic observation. Briefly, treated blood smear was dried and working Leishman stain was used to stain the blood smear. Excess stain was washed out with distilled water and slides were dried and observed and microphotographs were taken by using a CCD camera attached microscope (Labomed LX300).[26]

2.8 Antioxidant activity: DPPH spectrophotometric assay for determination of free radical scavenging activity

DPPH assay for antioxidant activity analysis is an easy, rapid and sensitive way to survey the antioxidant activity of a molecule.[33] From the stock of the DPPH solution (0.2 mM), a volume of 0.5 mL was mixed with the sample solutions at different concentrations (30–270 μg mL^{-1}). The concentrations of AuNP used are 30, 90, 150, 210 and 270 μg mL^{-1}. Control was prepared containing methanol and DPPH solution. In another experimental set, a sequence of reaction mixture containing 10–100 μg mL^{-1} ascorbic acid in methanol was used as the standard. All solutions were incubated for 30 min at room temperature in dark. Absorbance was measured at 517 nm wavelength. The percentage of radical scavenging by the samples was calculated as

$$\%\ \text{inhibition} = \frac{A_{\text{control}} - A_{\text{test}}}{A_{\text{control}}} \times 100$$

Here, A = absorbance.

2.9 Antibacterial sensitivity assay of gold nanoparticle

Both types of gold nanoparticles (citrate stabilized and leaves extract stabilized) were tested for the antibacterial activity by using disc diffusion methods.[34] Briefly, the stock solutions (328 μg mL^{-1} for both) were diluted to concentrations of 2.5, 5, 10, 20, 50 and 100 μL mL^{-1} of AuNP in water. 20 μL of each dilution was impregnated into sterile, blank discs 6 mm in diameter. A 5 μL of AuNP solution was spotted alternately on both sides of the discs and allowed to dry before the next 5 μL was spotted to ensure precise impregnation. All discs inoculated with Muller Hinton Agar media (MHA) plates were fully dried before the application of bacterial lawn. Turbidity of bacterial strain *viz.*, *Staphylococcus aureus*, *E. coli*, *Enterococcus* was adjusted to∼10 CFU mL^{-1} (corresponding to 0.5 Mc Farland standards). Antibiotic discs were placed on the media contained plates and pressed to ensure complete contact with agar. Prepared plates were incubated at 37 °C for 24–48 h. Standard antibiotics (Clindamycin, Gentamycin, Ampicillin) were used as positive control for bacteria. After completion of incubation time, the zone of inhibition was measured. Antimicrobial activity was evaluated by measuring the diameter of the inhibition zone (IZ) around the discs. The assay was repeated triplicate. Antibacterial activity was calculated as the mean zone of inhibition diameters (mm) produced by the AuNP solution.

2.10 Effect of *M. oleifera* stabilized gold nanoparticle in brain histological architecture

Swiss albino mice (weight 25–30 g) were used as the experimental animal model in the present study. All animal experimental procedures were performed in accordance with the 'Guidelines for Care and Use of Laboratory Animals' of Department of Zoology, Gauhati University, Assam, India and approved by the Institutional Animal Ethics Committee of Gauhati University, Assam, India. The animal experiments were completed as per the approval of the IAEC, Gauhati University, Assam, India. The mice were caged at usual 12 : 12 hours light dark cycles with usual diet and water *ad libitum*. Daily handling of the animals was maintained to reduce the stress. Animals were divided into two groups (one citrate capped gold nanoparticle administered and another one administered with *M. oleifera* stabilized gold nanoparticle) along with one control group fed with normal saline. Each group contained five mice. Mice were administered at the dose of 0.025 mM of gold nanoparticle per day for one week. After one week of continuous gold nanoparticle administration animals were sacrificed and brain tissues were collected. Tissues were fixed in Carnoy's fixative.[35] The fixed tissues were embedded in paraffin wax for histological study. Histological sections were prepared at 5 μm thickness using the laboratory rotary microtome. Sections were stained with haematoxylin and eosin (H & E stain) using standard procedure[36] and observed under microscope.

2.11 Photo-catalytic activity: photo-degradation of methylene blue dye

The photo-catalytic activity of the gold nanoparticles was screened on the degradation ability of methylene blue (MB) dye according to the method of Nur Syahirah Kamarudin *et al.* (2017).[37] Basically, methylene blue has two characteristic UV-Vis absorption peak, one near 664 nm which comes from MB monomer,[38] whereas another shoulder peak near 612 nm arises due to MB dimer.[39] The first peak is associated with the conjugation between two dimethylamine substituted aromatic groups through sulfur and nitrogen atom of MB. The spectrum possesses two additional band in UV region near 245 and 292 nm originating from the substituted benzene.[38] Briefly, 3×10^{-2} M (1%) methylene blue dye was used as stock solution for the experiment. Five different concentrations (1×10^{-3}, 2×10^{-3}, 3×10^{-3}, 4×10^{-3}, 5×10^{-3} M) of gold nanoparticles was used as working solution and mixed well with 200 μL of methylene blue dye solutions using a vortex mixture for 30 min in dark environment to attain the adsorption–desorption equilibrium on the surface of catalyst. The reaction was carried out under light irradiation for 3 h. A suspension of 2–3 mL was collected to assess the photo-catalytic degradation of dye at specific time intervals. Finally, the reaction mixtures were centrifuged at 13 000 rpm for 10 min before being analysed by UV-Vis spectrophotometer at wavelength of 664 nm. The reduced intensity of the principal absorption band signifies the decrease in dye concentration in the solution which in turn leads to the extent of dye adsorption. Degradation of methylene blue was calculated using the following formula as percentage degradation:

$$\%\ \text{degradation} = \frac{A_0 - A_t}{A_0} \times 100$$

where A_0 is the initial absorbance of dye solution and A_t is the absorbance of dye solution after photo-catalytic degradation.

3 Results and discussion

Gold nanoparticles were successfully synthesized from gold chloride salt ($HAuCl_4 \cdot 3H_2O$), stabilized by plant extract and

compared with conventionally synthesized citrate stabilized gold nanoparticles. The resultant nanoparticles were characterized by visual color change, UV-Vis spectra, photoluminescence spectra, DLS measurement, FTIR spectra, TEM images. Finally, they were employed to find *in vitro* antioxidant, antimicrobial, blood cytotoxicity and photo-catalytic activities.

3.1 Characterization

A. Characterization of methanolic extract of leaves of *M. oleifera*. The methanolic extract of the leaves of *M. oleifera* was employed to various spectroscopic tools to characterize. The phytochemicals present in the extract was determined using qualitative test following some reported methods as described in ESI.† From the analysis, the extract was found to be contained with alkaloids, flavonoids, terpenoids, polyphenols, glycoside *etc.* as shown in Fig. S1A in ESI.† Similarly, the FTIR and UV-Vis spectra of the methanolic extract were also recorded and put in the Fig S1(B and C) in ESI† with complete discussion.

B. Characterization of citrate stabilized gold nanoparticles (gnp-citrate). Citrate stabilized gold nanoparticles were prepared following a standard protocol given by Chayanika Devi *et al.* (2016) as described above.[26] So formed nanoparticles were characterized by various spectroscopic techniques. Dynamic light scattering (DLS) measurement performed, showed that the nanoparticles dispersion contains maximum gold nanoparticles of size 20–30 nm (Fig. 1A). DLS data regarding nanoparticles size is also confirmed by TEM image (Fig. 1B) which indicates the presence of particles of size 15–20 nm. A high resolution TEM image has been added in Fig. S2A of ESI† which confirms almost equal size nanoparticle formation. DLS size (hydrodynamic size) is always slightly bigger than TEM size. The SEM image was also recorded to get the size and morphology of the gold nanoparticles which resembles with TEM size as shown in Fig S3A of ESI.† The elemental mapping was done with SEM EDAX technique and presence of gold, oxygen, carbon was observed (Fig. S3B†). The elemental% was put at the inset of Fig. S3B.† The XRD pattern also indicates the formation of crystalline gold nanoparticles, represented by four standard Bragg reflection at 38.3 (111), 44.4 (200), 64.5 (220) and 77.5(311) of face centered cubic lattice (Fig. 1C). The intense peak at 38.1 reveals preferential growth of the nanoparticles in (111) direction.[40] The obtained XRD pattern is resembled with the JCPDS data (00-004-0784) supporting gold nanoparticle formation. It describes that the gold nanoparticles have face centred cubic (fcc) structure. The edge length (a) of the cubic unit cell is 4.0789 Å as noted from the data. The cell volume (D) for each unit cell is 67.85. The distances of two adjacent crystal planes (d spacing) in the lattice of the fcc structures are calculated to be 2.3555, 1.44, 2.039 and 1.229 Å for (111), (220), (200) and (311) planes respectively. UV-Vis spectrum (Fig. 1D) clearly reveals the peak of standard gold nanoparticles near 535 nm forming due to surface plasmon resonance of gold nanoparticles. The functionalities present on the surface of the citrate capped gold nanoparticles are found from the FTIR spectrum shown below (Fig. 1E). It consists of –O–H (3452 cm^{-1}), –C–H (2922 cm^{-1}), –C═O (1630 cm^{-1}) functional group which is coming from the citrate group stabilizing the gold nanoparticles. Surface charge on the citrate stabilized gold nanoparticles was found to be −31 mV (Fig. S6A†) as shown in the ESI.†

C. Characterization of *M. oleifera* stabilized gold nanoparticles (GNP). Biosynthesis of gold nanoparticles was

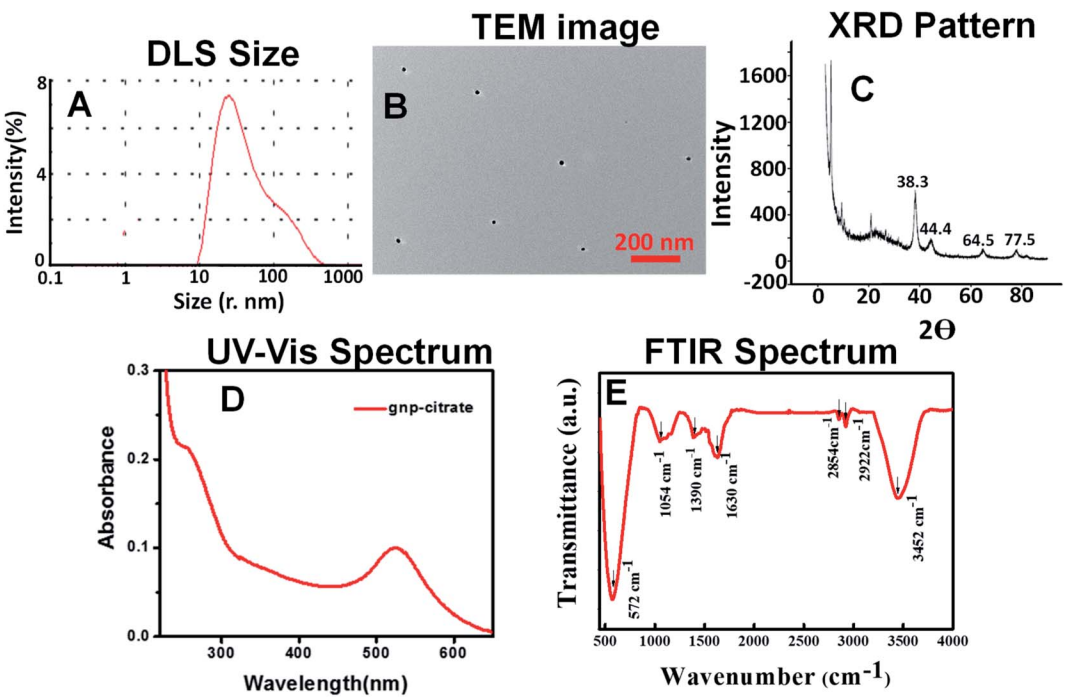

Fig. 1 (A) DLS size (B) TEM image (C) XRD pattern (D) UV-Vis spectrum (328 g mL^{-1} aqueous solution) (E) FTIR spectrum of gnp-citrate.

performed using gold chloride ($HAuCl_4 \cdot 3H_2O$) and methanolic mature leaf extract of *M. oleifera* as the stabilizing agent. A number of characterization tools were employed on those nanoparticles. DLS measurement revealed that the nanoparticles dispersion contains maximum gold nanoparticles of size bellow 30 nm as shown in Fig. 2A. TEM image (Fig. 2B) also gives particles of size 14–30 nm. A high resolution TEM image is included in the Fig. S2B.† As the nanoparticles contains a wide range of size, its particle size distribution plot was made from TEM analysis and put in the Fig. S2C† for clarification. The plot implies that majority of the particles falls in the range of 17–27 nm. The size and morphology of the gold nanoparticles was also observed from the SEM image which correlates with the TEM size as shown in Fig S3C of ESI.† The elemental mapping collected from SEM EDAX technique showed the presence of gold, oxygen, carbon in the sample (Fig. S3†). It is observed that the carbon content in this case is higher than the gnp-citrate as observed from the SEM EDAX data indicating the presence of the extract on AuNPs. The elemental% was put at the inset of Fig. S3D.† XRD pattern (Fig. 2C) was also recorded to get standard gold nanoparticle characteristic 2θ value for the gold nanoparticle which confirms the formation of crystalline gold nanoparticles. This XRD pattern is matched with the JCPDS data (00-004-0784) supporting gold nanoparticle formation. It describes that the gold nanoparticles have face centred cubic (fcc) structure. XRD pattern is similar to citrate stabilized crystalline gold nanoparticles as explained above, represented by four standard Bragg reflections, predominating at 2θ value of 38.1 which clearly leads to preferential growth of the nanoparticles in (111) direction.[40] The intense peak at 38.1 reveals preferential growth of the nanoparticles in (111) direction. The edge length (a) of the cubic unit cell of the fcc structure is 4.0789 Å as noted from the data. The cell volume (D) for each unit cell is 67.85. The distances of two adjacent crystal planes (d spacing) in the lattice of the fcc structures are calculated to be 2.3555, 1.44, 2.039 and 1.229 Å for (111), (220), (200) and (311) planes respectively. The UV-Vis absorption spectra of *M. oleifera* stabilized gold nanoparticle, synthesized at different conditions are shown in the below Fig. 2D. It is seen that strong absorbance peak near wavelength of 540 nm, which indicate the presence of gold nanoparticles. Slight blue shift in the peak position owes to decrease in particle size which could be attributed to the confinement effects.[41] The FTIR spectrum shown in Fig. 2E is found to be consisted of –O–H (3411 cm^{-1}), –C–H (2928 cm^{-1}), –C═O (1660 cm^{-1}) functional groups. These may come from the leaves extract containing various biomolecules as explained on the surface of the gold nanoparticles.[42] Surface charge on the green gold nanoparticles was found to be −15.7 mV (Fig. S6B†) as shown in the ESI.†

3.2 Determination of band gap energy and stability of citrate stabilized and *M. oleifera* stabilized gold nanoparticles

For the stability of the synthesized nanoparticles, UV-Vis spectra were recorded for each sample and their change of the surface plasmon peak at wavelength near 525–540 nm was monitored at certain interval of time (0, 15, 30 days) as shown in Fig. 3, S4 and S5 (ESI†) respectively. Each figure consists of four sub figures (a–d) representing UV-Vis spectra of gold nanoparticles stabilized with citrate (a), immature leaf (b), mature leaf (c), old age leaf (d). It is reported that variation in the properties of metal nanoparticles is dependent on the shifting of the surface plasmon peak position as well as its intensity.[43] It was observed

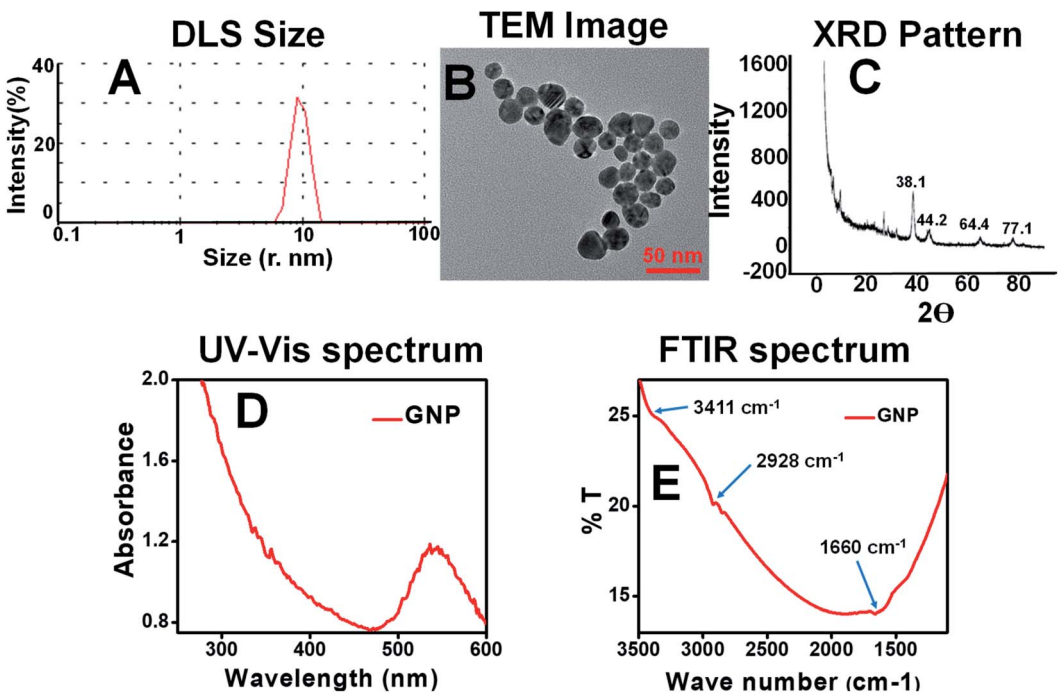

Fig. 2 (A) DLS size (B) TEM image (C) XRD pattern (D) UV-Vis spectrum (328 μg mL^{-1} aqueous solution) (E) FTIR spectrum of GNP.

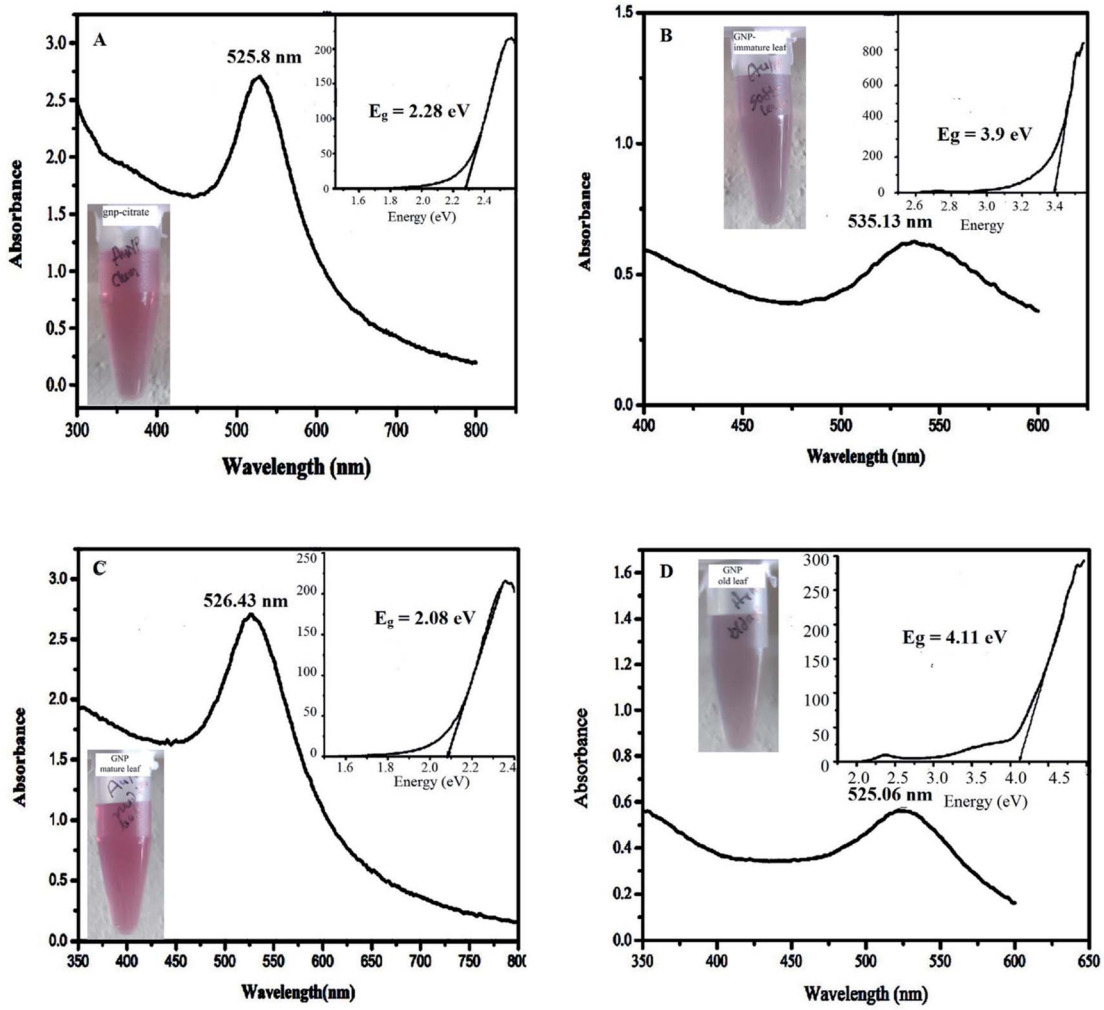

Fig. 3 UV-Vis spectra of AuNP just after the synthesis, stabilized by (A) citrate (B) immature leaf (C) mature leaf (D) old age leaf (inset: the visual color and Tauc plot to determine direct band gap energy of respective samples).

from the UV-Vis spectra for all samples, almost stable surface plasmon peak (in terms of shifting and intensity) was found for the gold nanoparticles stabilized by mature leaves compared to other three which clearly infers the persistence of the nanoparticles through the time without agglomeration. It can be mentioned here that red shifting occurs in the surface plasmon peak of metal nanoparticles when agglomeration takes place.[44] The visual appearance of the synthesized gold nanoparticles stabilized by different agents are shown in the inset of respective UV-Vis spectra in Fig. 3(A–D) just after synthesis. It indicates that all the samples contain standard color of gold nanoparticle *viz.* purple to pink.

Stability is also related to band gap energy (E_g) calculation.[31] Band gap is reported to be associated with incident photon energy to the sample in the UV-Vis spectra measurement through a relationship known as Tauc equation.[30] As explained in the method section, the E_g can be obtained from *hv versus* $(\alpha h\nu)^2$ plot (also called as Tauc plot) making tangent to the curve at the point of maximum slope and extrapolating to $(\alpha h\nu)^2 = 0$. The insets of the Fig. 3, S4 and S5† denote the Tauc plot for each nanoparticles showing the band gap energy, E_g. The optical band gap (E_g) is found for the citrate stabilized AuNP as 2.08 eV (inset of Fig. 3A) and after 15 days of interval 2.09 eV (inset of Fig. S4A†) and after 30 days of interval 2.12 eV (inset of Fig. S5A†). The optical band gap (E_g) is found for the green (immature leaf) AuNP as 3.9 eV (inset of Fig. 3B), after 15 days of interval 3.95 eV (inset of Fig. S4B†) and after 30 days of interval no band gap was observed (inset of Fig. S5B†). The optical band gap (E_g) is found for the green (mature leaf) AuNP as 2.08 eV (inset of Fig. 3C) and after 15 days of interval 2.08 eV (inset of Fig. S4C†) and after 30 days of interval 2.13 eV (inset of Fig. S5C†). The optical band gap (E_g) is found for the green (old aged leaf) AuNP as 4.11 eV (inset of Fig. 3D) and after 15 days of interval 3.53 eV (inset of Fig. S4D†) and after 30 days of interval no band gap was observed (inset of Fig. S5D†). The results suggest that the gold nanoparticles stabilized with matured leaves have band gap energies similar to citrate stabilized gold nanoparticles which is reported to be stable.[45]

From the above two analyses, it is found that the gold nanoparticles, stabilized with matured leaves give more stable

absorption peak compared to the other two green nanoparticles with immature and old leaves. Even, the matured leaves give similar UV-Vis spectrum and stability along with band gap energy in comparison to the citrate stabilized gold nanoparticle. A combined UV-Vis spectra for mature leaves derived GNP at different time interval has been incorporated in the Fig. S6† of ESI for comparative purpose. The figure depicts that the surface plasmon peak of the same GNP is consistent with time.

Moreover, the stability of green gold nanoparticles was also analysed in terms of pH variation keeping the other parameter constant. The results were put in the ESI (Fig. S7–S9†). From the data, it is noted that gold nanoparticles formed at pH 6 are more stable than other two pH (3.4 and 9.6).

As the green synthesis of gold nanoparticles can produce stable products as evident from the time and pH dependent studies, it is of utmost important to find out the mechanistic insight of the nanoparticle formation.

In case of chemical synthesis (gnp-citrate), precipitation method is used with the help of a reducing agent (here trisodium citrate). Here, the precursor is gold salt ($HAuCl_4$) producing Au^{3+} ion which is reduced first to Au^{1+} (initial reduction) and then to Au^0 (second reduction) by citrate group. Basically, the reduction is followed by forming clusters and then transforming into larger polycrystalline particles through aggregation.[46] According to one earlier report, the growth process is explained in terms of first formation of clusters of size 2.5 nm which gets assembled into chains and networks of crystalline particles interconnected by amorphous gold of size 4 nm.[47] The diameter of the chain increases and finally collapses near 7 nm size to form smaller particles. Similarly, growing process of small particles continues in cyclic fashion. pH dependent formation has also been illustrated consisting of two to three steps like nucleation, diffusion-controlled growth and intraparticle ripening.[48]

The study with advanced instruments on particle growth suggests that the factors influencing the growth process are the reaction temperature and the initial concentration of gold precursor which accelerate the particle formation process significantly on increasing.[49]

In case of biosynthesis (GNP), the initial reduction step of Au^{3+} to Au^0 is offered by the different phytochemicals present in the plant extract like phenolic, alkaloid, flavonoid, enzymes, proteins *etc.* They also work as stabilizing agent for the developed nanoparticles. Here, no citrate is applied for reduction and hence it is a green material.

Other process of growth is similar to chemical synthesis. It reduces the use of hazardous chemicals there by making the process cheap.

The reducing capacity of polyphenols, organic acids, and proteins are well established and hence, the extract is expected to show synergistic effect with all the phytochemicals.[50] Meanwhile, no exact mechanism is reported so far regarding the plant extract-based nanoparticle synthesis. But importance of biosynthesis of nanoparticles using plant extract stems from the advantages of producing large quantity without contamination and energetically favourable spherical shape.[51]

3.3 Antioxidant activity analysis of the synthesized gold nanoparticle

The antioxidant activity of both citrate stabilized AuNP and green AuNP was evaluated by DPPH free radical scavenging assay and their antioxidant activities are represented in Fig. 4. The IC_{50} value of citrate stabilized AuNP (IC_{50} = 2.33 μg mL^{-1}) is more than the methanolic leaf extract of *M. oleifera* mediated green AuNP (IC_{50} = 1.9 μg mL^{-1}). Therefore, the green AuNP has more free radical scavenging activity, (thus, the antioxidant activity) in comparison to the citrate stabilized AuNP. In fact, the recent report on aqueous extract of *M. oleifera* leaves assisted gold nanoparticles synthesis revealed that it has higher IC_{50} value (60 μg mL^{-1}) than our system indicating the effectiveness of our proposed system in free radical scavenging activity.[20] The attachment of the plant component in the green nanoparticle might be the modulating factor for the enhanced antioxidant activities of the green nanoparticle over the citrate stabilized gold nanoparticle.[13]

3.4 Antimicrobial activity of gold nanoparticle

The antimicrobial activities of both citrate stabilized and green synthesized AuNP were investigated using disc diffusion

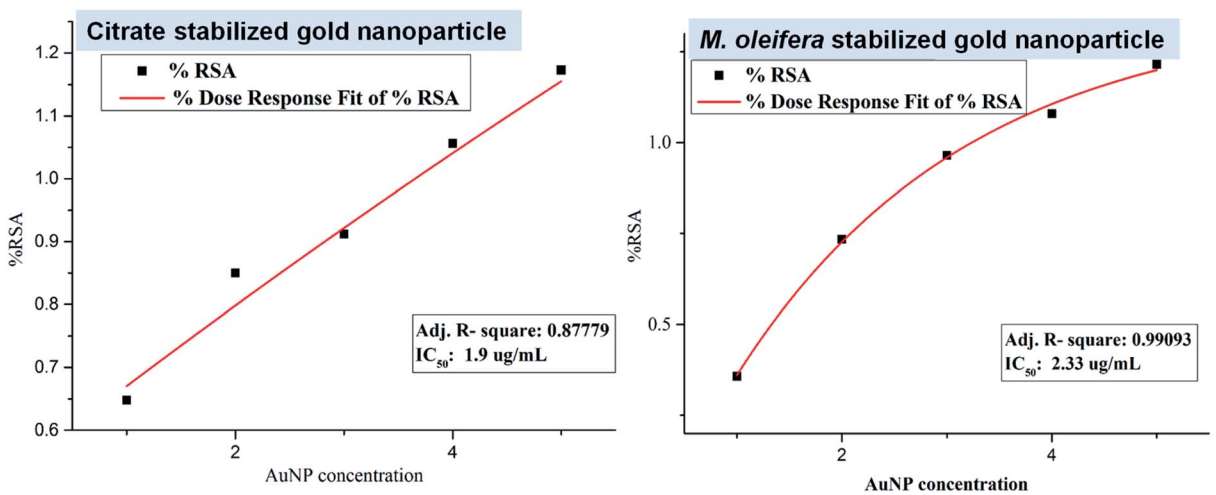

Fig. 4 The plots for the free radical scavenging activity (RSA) assay of citrate stabilized AuNP and green synthesized AuNP.

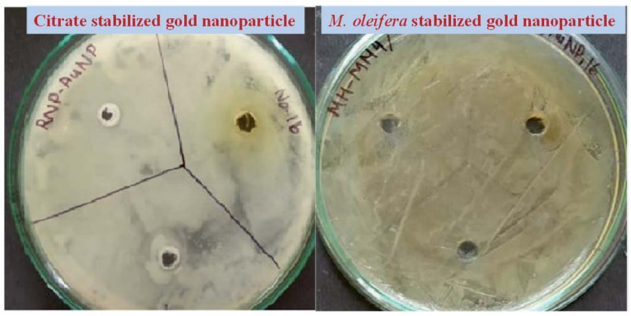

Fig. 5 Antibacterial sensitivity assay of the citrate and green stabilized AuNP against *Staphylococcus aureus, E. coli, Enterococcus* by disk-diffusion technique. No significant Zone of Inhibition (ZoI) was observed against the bacterial strain by both type of particle.

method against *Staphylococcus aureus* (Gram positive bacteria), *E. coli* (Gram negative bacteria), *Enterococcus* (Gram positive bacteria). Both the studied sample showed no significant antimicrobial activity against *Staphylococcus aureus*, *E. coli*, *Enterococcus* (Fig. 5) thus, from the antibacterial activity assay by disc diffusion method it is observed that the AuNP in this size range and with these surface characteristics are unable to show any lethality to the *Staphylococcus aureus*, *E. coli*, *Enterococcus* culture. Previous studies report that established antiepileptic drugs like gabapentin, car azepine, Lobazam, Lonazep, Lametec *etc.* could show no antibacterial property against the pathogenic bacteria or could show little activity at higher dose only.[52,53] Only valproic acid shows antibacterial property against the pathogenic bacteria.[53] But as an antiepileptic drug, valproic acid shows some individual specific side effects like vomiting, headache, drowsiness, *etc.*54 Thus, from these studies, it can be concluded that good antiepileptic drug does not show antimicrobial properties against the pathogenic bacterial isolates. No response to bacterial isolates by the gold nanoparticles both citrate stabilized and *M. oleifera* stabilized gold nanoparticle may be a criterion to the neuroactive potentialities of the green nanoparticle along with its other characteristics. So, it may be indicative that a neuroactive molecule is unable to show harm towards bacteria or *vice versa*. The exact reason is not known yet. However, gold nanoparticles synthesized with *A. muricata* leaf extract was reported to show significant antibacterial activity against a number of bacteria in the order of *S. aureus* > *Enterococcus* > *K. pneumonia* > *C. sporogenes*.[55] Hence, other plant leaves extract derived gold nanoparticles other than *M. oleifera* may have antimicrobial activity. But the leaves extract from *M. oleifera* has not been studied yet for this purpose and our report suggests the incapable nature of *M. oleifera* to impart the antibacterial activity into the gold nanoparticles.

Table 1 Haemolysis (%) caused by citrate stabilized and green AuNP in blood cells in concentration when incubated for 90 minutes[a]

AuNP concentration	Haemolysis (%) caused by citrate stabilized AuNP	Haemolysis (%) caused by green AuNP
0.25 μL mL^{-1}	22.9683 ± 0.015	5.116 ± 0.02
0.50 μL mL^{-1}	33.5274 ± 0.016	8.069 ± 0.04
1.0 μL mL^{-1}	85.773 ± 0.020	10.399 ± 0.02
2.5 μL mL^{-1}	93.4276 ± 0.050	24.5424 ± 0.04
5.0 μL mL^{-1}	112.22 ± 0.200	45.5906 ± 0.40

[a] Data are represented as mean ± SD, each experiment was performed in triplicate and samples were from five subjects.

3.5 Evaluation of cytotoxic effect of AuNP on blood cells – an *in vitro* assay

Cytotoxic effect was evaluated for both nanoparticles. Table 1 shows blood cells are found to be affected by AuNP as increasing in dose in both cases for citrate and green stabilized process. The lower concentration (*i.e.* 0.25 and 0.50 μL mL^{-1}) of AuNP treatment shows no significant haemolytic activity (when the spectrophotometric data were statistically analysed) in comparison to the comparatively higher concentration (1.0, 2.5 and 5.0 μL mL^{-1}) in blood cells which are statistically significant ($p < 0.01$). It also reveals that green AuNP are less cytotoxic in comparison to the citrate stabilized. The green synthesized AuNP are seen to be more biocompatible in nature at its lower concentration than the citrate stabilized AuNP.

Micro photographic analysis of blood cells reveals swelled blood cells as shown in Fig. 6 (indicated by white arrow) when treated with AuNP. Deformative blood cells are found less numbered in low concentration treatment in comparison to the higher concentration treatment. It is also obvious from the figure that density of blood cells is decreasing with increasing concentration of AuNP treatment. In all cases, green nanoparticle treatment shows less harmful affect in comparison to the citrate stabilized AuNPs. The AuNP can penetrate the cell membrane *via* the receptor mediated endocytosis pathway into the blood cells because of its surface and size characteristics. Ionic strength of the biological system favours the nanoparticle aggregation *via* the electrostatic interaction with the system. After AuNP entry in the blood cells above a critical concentration causes aggregation and flocculation inside the cells which may be the cause of the swelling and deforming blood cells resulting in haemolysis of the cells which is reflected in the haemoglobin concentration in the reaction mixture.[26] Green nanoparticle shows better result in terms of haemolysis *i.e.* less haemolysis in comparison to the citrate stabilized AuNP. Citrate stabilized nanoparticles are synthesized completely by chemical entity; on the other hand, the green nanoparticle contains a natural product component. Therefore, because of the presence of the green component it is supposed to be less cytotoxic *i.e.* less harmful.[56] The lesser haemolytic effect of green gold nanoparticles with respect to chemically synthesized gold nanoparticles was also reported earlier. An ethanolic extract of *Curcuma manga* synthesized AuNP was found to show lower haemolytic effect against RBC compared to CTAB (cetyltrimethylammonium bromide) based AuNP. The percentage of haemolysis were found to be 2.7%, 1.8%, 2.6%, 6.2%, and 9.9% with that AuNPs having concentrations of 3.13, 6.25, 12.50, 25.00, and 50.00 μg mL^{-1}, respectively. Whereas, the CTAB stabilized AuNPs with concentrations 25.00 and 50.00 μg mL^{-1}

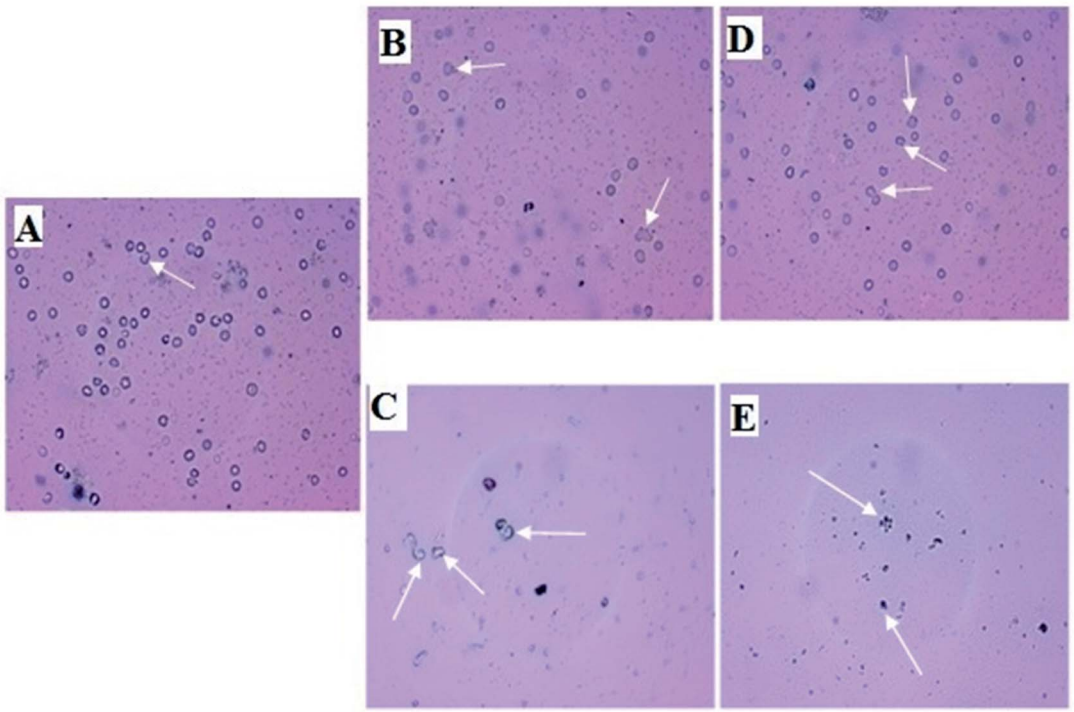

Fig. 6 Micro photographic view of blood cells treated with different concentration of citrate and green AuNP along with negative and positive control samples. Deformations are indicated by white arrows. Blood cells treated with (A) PBS (B) low concentration (0.25 μL mL^{-1}) of citrate stabilized AuNP (C) high concentration (5.0 μL mL^{-1}) of citrate stabilized AuNP (D) low concentration (0.25 μL mL^{-1}) of green AuNP (E) high concentration (5.0 μL mL^{-1}) of green AuNP. Negative control sample treated with SDS shows complete haemolysis without any residual blood cells. Here, only low and highest treatments are shown as indicative.

showed 44.7% and 96.0% of haemolysis. Even the microscopy images imply that the RBC aggregation/deformation took place with the CTAB based AuNPs which was absent in case of *Curcuma manga* synthesized AuNP.[57]

3.6 Effect of *M. oleifera* stabilized gold nanoparticle in brain histological architecture

In Fig. 7, plate A (brain section of normal mice) shows the features of brain with normal histological architecture with no lessions. In plate B (brain section of citrate stabilized AuNP treated mice), the parenchymatous cells of the cerebral cortex region are seen degenerated and featured vacuolation is clearly seen with neuronal cell detoriation. Edemic cells are observed due to injured cells. Pyknotic nuclei of glial cells are observed. Infiltration of inflammatory cells is seen in a region within cerebral neocortex I and II region. In plate C (brain section of *M. oleifera* stabilized AuNP treated mice) brain appears with fewer lesions and tissue damage appears to be minimized. Edematous tissues are lessened to a greater extent. Regeneration of neuronal cells is observed which is nearer to the normal tissues. Gold nanoparticle within the size range of 12 nm to 50 nm can finely be distributed in the brain.[58] The blood brain barrier can interact with the gold nanoparticle causing its entry to the brain. But citrate stabilized gold nanoparticle induces some marked neurotoxicity by accessing the brain parenchymal cells with the nanoparticles[59] which is also evidenced by our study (plate B). But in case of *M. oleifera* stabilized gold nanoparticle treated mice group histological alterations are less observed which may be its green component as well as for the neuroprotective efficacy of methanolic fraction of *M. oleifera* leaf extract. In literature histological study of green gold nanoparticles in brain tissue not reported. However, the effect of green AuNPs in other cells of the body like kidney, liver and testis and dose dependent toxicity or deformation of cell histological architecture are reported. The *Fusarium oxysporum* fungus derived green AuNPs was found to be mild change inducer for liver and kidney cells in nontoxic doses, while it imparts no change in Testis.[60]

3.7 Photo-catalytic activity: photo-degradation of methylene blue dye

Five different concentrations (1×10^{-3}, 2×10^{-3}, 3×10^{-3}, 4×10^{-3}, 5×10^{-3} M) of gold nanoparticles was used as working solution and mixed well with 200 μL of methylene blue dye solutions (3×10^{-2} M or 1%) using a vortex mixture for 30 min in dark environment as explained in experimental part. Then light irradiation of the suspension for 3 h followed by centrifugation at 13 000 rpm for 10 min gave supernatant which on UV-Vis spectrophotometer, showed some absorbance value at wavelength 664 nm. Then putting that value of concentration A_t (calculated from absorbance) in the respective formula, degradation percentage was obtained with respect to initial

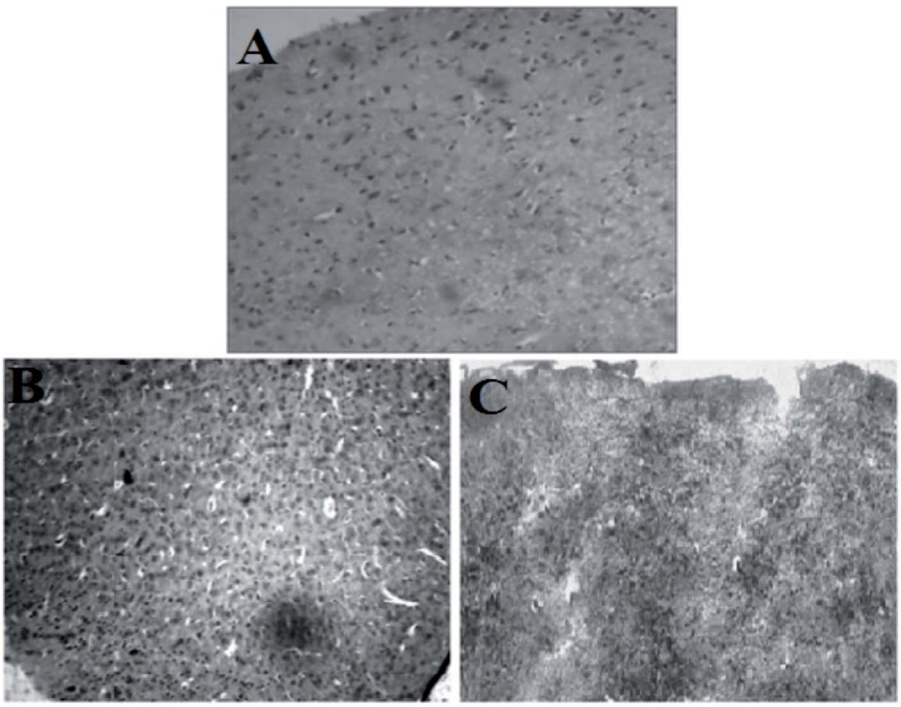

Fig. 7 Histological architecture of mice brain tissue (whole cerebral cortex region): (A) normal brain, (B) citrate stabilized AuNP treated brain, (C) *M. oleifera* stabilized treated brain.

concentration of MB (A_0). Here, plot of $\ln(A_t/A_0)$ *vs.* reaction time was shown for each sample in Fig. 8A and B. MB degradation shown by citrate stabilized gold nanoparticles is represented in Fig. 8A whereas degradation by green gold nanoparticles (GNP) is shown in Fig. 8B. From both figures, it is noted that higher the concentration of gold nanoparticles, higher is the MB degradation. But degradation is higher for green gold nanoparticles compared to citrate stabilized gold nanoparticles. It was monitored at certain time interval (10, 20 and 20 min) and data were compared with respect to the control MB solutions, denoted as "i" performed for both AuNPs as shown in Fig. 8A and B. Similar behaviour was also observed for green tea leaves extract derived gold nanoparticles earlier.[61] There, the photoreduction of methylene blue by green gold nanoparticles was found to be higher than the case where no nanoparticles was present. The time taken for methylene blue (5×10^{-5} M) degradation by the green gold nanoparticles was recorded to be 3 min. However, our green AuNP is not yet used for photocatalytic activity so far.

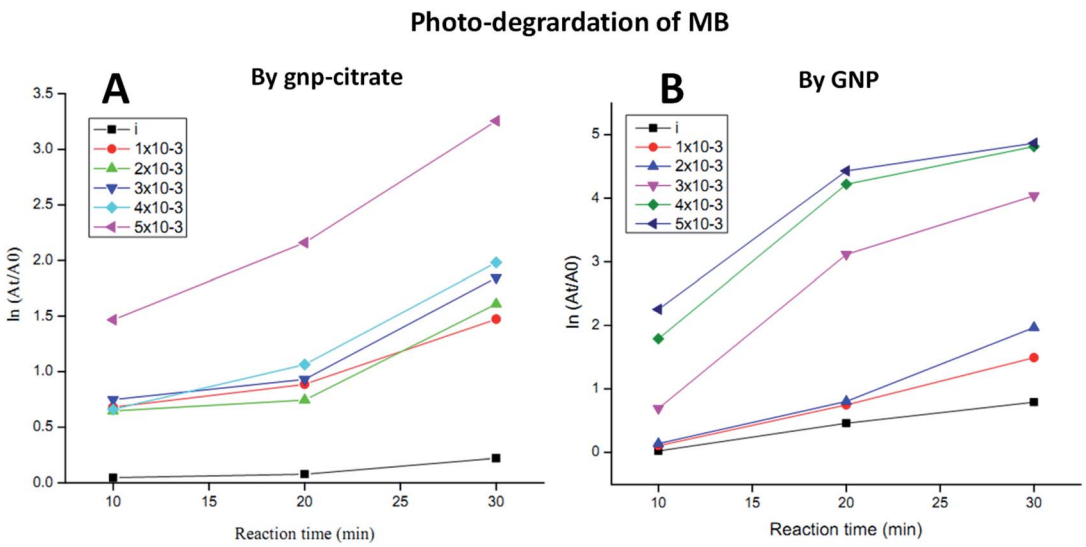

Fig. 8 Photocatalytic degradation plots of MB by (A) gnp-citrate and (B) GNP.

4 Conclusions

In this work, a systematic investigation was carried out to find the physiochemical as well as biological activity of gold nanoparticle stabilized by conventional citrate and that stabilized by *M. oleifera* plant leaves extract. From the present study, it can be concluded that methanolic leaf extract of *M. oleifera* can be used as a stabilizing agent in the synthesis of an effective and stable gold nanoparticle with superior properties which have tremendous usability in biomedical science research. It was observed that *M. oleifera* leaves extract stabilized gold nanoparticles were found to be biologically more active. The green gold nanoparticles prepared using *M. oleifera* show less cytotoxicity and helps in regeneration of neuronal cells in animal model study. The high medicinal values of the biomolecules present in the methanolic fraction of this plant leaves contribute to the observed activities.[62] Moreover, gold nanoparticles stabilized by *M. oleifera* extract also show better photocatalytic properties in degradation of MB. This may come from the polyphenolic compounds present in the extract having electron rich environment. So, this method of gold nanoparticles synthesis will open a new avenue for synthesis of biologically active gold nanoparticle.

Author contributions

PK: conceptualization, methodology, supervision, review and editing; DC: supervision, visualization, methodology, data analysis, review and editing; PVBR: conceptualization, methodology and editing; MB: visualization, methodology, data analysis, review and editing; JSB and CD: investigation, analysis, review and editing; UH: investigation, analysis.

Conflicts of interest

There are no conflicts to declare.

Acknowledgements

Authors acknowledge the authorities of Advanced Level Institutional Biotech Hub (Phase – II) of Pub Kamrup College, Guwahati, India supported by Department of Biotechnology, Govt. of India for giving full facilities for performing the experiments on nanoparticle synthesis, chemical and biological activities. The authors thank Central Instrumental Facility of Institute of Advanced Studies in Science and Technology for helping with various instrumentations.

References

1 M. C. Daniel and D. Astruc, *Chem. Rev.*, 2004, **104**, 293–346.
2 U. Baruah, N. Gogoi, A. Konwar, M. J. Deka, D. Chowdhury and G. Majumdar, *J. Nanopart.*, 2014, DOI: 10.1155/2014/178518.
3 M. J. Deka and D. Chowdhury, *ChemistrySelect*, 2017, **2**, 1999–2005.
4 S. Majumdar, T. Bhattacharjee, D. Thakur and D. Chowdhury, *ChemistrySelect*, 2018, **3**, 673–677.
5 S. Shrivastava and D. Dash, *J. Nanotechnol.*, 2009, **14**, 184702, DOI: 10.1155/2009/184702.
6 J. S. Boruah and D. Chowdhury, *ChemistrySelect*, 2019, **4**, 4347–4354.
7 J. S. Boruah and D. Chowdhury, *Appl. Nanosci.*, 2020, **10**, 2207–2218, DOI: 10.1007/s13204-020-01374-2.
8 M. C. Senut, Y. Zhang, F. Liu, A. Sen, D. M. Ruden and G. Mao, *Small*, 2016, **12**, 631–646.
9 E. H. Ismail, A. M. A. Saqer, E. Assirey, A. Naqvi and R. M. Okasha, *Int. J. Mol. Sci.*, 2018, **19**, 2612.
10 J. S. Boruah, P. Kalita, D. Chowdhury and M. Barthakur, *Mater. Today: Proc.*, 2021, **46**, 6404–6408.
11 J. S. Boruah, P. Kalita, D. Chowdhury and M. Barthakur, *Mater. Today: Proc.*, 2021, DOI: 10.1016/j.matpr.2021.06.172.
12 Y. Yulizar, T. Utari, H. A. Ariyanta and D. Maulina, *J. Nanomater.*, 2017, DOI: 10.1155/2017/3079636.
13 V. V. Makarov, A. J. Love, O. V. Sinitsyna, S. S. Makarova, I. V. Yaminsky, M. E. Taliansky and N. O. Kalinina, *Acta Naturae*, 2014, **6**, 35.
14 B. Sadeghi, M. Mohammadzadeh and B. Babakhani, *J. Photochem. Photobiol., B*, 2015, **148**, 101–106, DOI: 10.1016/j.jphotobiol.2015.03.025.
15 P. E. Cardoso-Avila, R. Patakfalvi, C. Rodriguez-Pedroza, X. Aparicio-Fernandez, S. Loza-Cornejo, V. Villa-Cruz and E. Martınez-Cano, *RSC Adv.*, 2021, **11**, 14624–14631.
16 G. K. Deokar and A. G. Ingale, *RSC Adv.*, 2016, **6**, 74620–74629.
17 J. O. Popoola and O. O. Obembe, *J. Ethnopharmacol.*, 2013, **150**, 682–691.
18 A. Leone, A. Spada, A. Battezzati, A. Schiraldi, J. Aristil and S. Bertoli, *Int. J. Mol. Sci.*, 2015, **16**, 12791–12835.
19 M. Vergara-Jimenez, M. M. Almatrafi and M. L. Fernandez, *Antioxidants*, 2017, **6**(91), DOI: 10.3390/antiox6040091.
20 M. S. Kiran, C. R. Rajith Kumar, U. R. Shwetha, H. S. Onkarappa, V. S. Betageri and M. S. Latha, *Chem. Data Collect.*, 2021, **33**, 100714.
21 D. Kaushik, S. L. Khokra, P. Kaushik, A. Saneja and D. Arora, *Pharmacologyonline*, 2009, **3**, 101–106.
22 D. Sivaraman and P. Muralidaran, *E-J. Chem.*, 2010, **7**(4), 1555–1561.
23 J. N. Amrutia, M. Lala, U. Srinivasa, A. R. Shabaraya and M. R. Samuel, *Int. Res. J. Pharm.*, 2011, **2**, 160–162.
24 P. Kalita, PhD thesis, Assam University, Diphu Campus, Assam, India, 2019.
25 W. G. Shousha, W. M. Aboulthana, A. H. Salama, M. H. Saleh and E. A. Essawy, *Bull. Natl. Res. Cent.*, 2019, **43**, 212, DOI: 10.1186/s42269-019-0221-8.
26 C. Devi, P. Kalita and M. Barthakur, *Mater. Today: Proc.*, 2016, **3**, 3439–3443.
27 H. Jia, X. Gao, Z. Chen, G. Liu, X. Zhang, H. Yan, H. Zhou and L. Zheng, *CrystEngComm*, 2012, **14**, 7600–7606.
28 A. Dzimitrowicz, P. Jamroz, G. C. diCenzo, I. Sergiel, T. Kozlecki and P. Pohl, *Arabian J. Chem.*, 2019, **12**, 4118–4130.

29 Y. Yulizar, T. Utari, H. A. Ariyanta and D. Maulina, *J. Nanomater.*, 2017, DOI: 10.1155/2017/3079636.

30 S. K. Santosh, F. P. Newhouse and J. M. Gregoire, *ACS Comb. Sci.*, 2016, **18**, 673–681.

31 N. Ghobadi, *Int. Nano Lett.*, 2013, **3**, 2.

32 A. Mishra, N. K. Kaushik, M. Sardara and D. Sahal, *Biointerfaces*, 2013, **111**, 713–718.

33 S. B. Kedare and R. P. Singh, *J. Food Sci. Technol.*, 2011, **48**, 412–422, DOI: 10.1007/s13197-011-0251-1.

34 A. W. Bauer, W. M. M. Kirby, J. C. Sherris and M. Truck, *Am. J. Clin. Pathol.*, 1966, **45**(4), 493–496.

35 P. Singhal, N. N. Singh, G. Sreedhar, S. Banerjee, M. batra and A. Garg, *J. Clin. Diagn. Res.*, 2016, **10**, 28–32.

36 M. Slaoui and L. Fiette, Histopathology Procedures: From Tissue Sampling to Histopathological Evaluation, in *Drug Safety Evaluation: Methods and Protocols*, ed. J. Gautier, Springer, 2nd edn, 2017, ch. 4, vol. 691, pp. 101–114.

37 N. S. Kamarudin, R. Jusoh, H. D. Setiabudi and N. F. Sukor, *Mater. Today: Proc.*, 2018, **5**, 21981–21989.

38 M. A. Rauf, M. A. Meetani, A. Khaleel and A. Ahmed, *Chem. Eng. J.*, 2010, **157**, 373–378.

39 N. M. Flores, U. Pal, R. Galeazzi and A. Sandoval, *RSC Adv.*, 2014, **4**, 41099–41110.

40 S. Krishnamurthy, A. Esterle, N. C. Sharma and S. V. Sahi, *Nanoscale Res. Lett.*, 2014, **9**, 627.

41 M. F. Zarabi and N. Arshadi, *Indian J. Clin. Biochem.*, 2013, DOI: 10.1007/s12291-013-0358-4.

42 P. V. Kumar, S. M. J. Kala and K. S. Prakash, *Mater. Lett.*, 2019, **236**, 19–22, DOI: 10.1016/j.matlet.2018.10.025.

43 A. Moores and F. Goettmann, *New J. Chem.*, 2006, **30**, 1121–1132.

44 C. Noguez, *J. Phys. Chem.*, 2007, **111**, 3806–3819.

45 S. Iravani, *Green Chem.*, 2011, **13**, 2638.

46 J. Kimling, M. Maier, B. Okenve, V. Kotaidis, H. Ballot and A. Plech, *J. Phys. Chem. B*, 2006, **110**, 15700.

47 B. K. Pong, H. I. Elim, J. X. Chong, W. Ji, B. L. Trout and J. Y. Lee, *J. Phys. Chem. C*, 2007, **111**, 6281.

48 X. H. Ji, X. N. Song, J. Li, Y. B. Bai, W. S. Yang and X. G. Peng, *J. Am. Chem. Soc.*, 2007, **129**, 13939.

49 J. Polte, T. T. Ahner, F. Delissen, S. Sokolov, F. Emmerling, A. F. Thunemann and R. Kraehnert, *J. Am. Chem. Soc.*, 2010, **132**, 1296–1301.

50 P. Dauthal and M. Mukhopadhyay, *Ind. Eng. Chem. Res.*, 2016, **55**, 9557–9577.

51 N. Noah, Green synthesis: Characterization and application of silver and gold nanoparticles in *Green Synthesis, Characterization and Applications of Nanoparticles*, ed. A. K. Shukla and S. Iravani, Elsevier, Amsterdam, 2019, ch. 6, pp. 111–135.

52 N. Esiobu and N. Hoosein, *Antonie Leeuwenhoek*, 2003, **83**, 63–68.

53 R. Nathiya, G. Mahalingam, I. Purushothaman, A. Vidya and K. Sangeetha, *J. Pharma Res.*, 2015, **4**(1), 13–15.

54 E. F. Dreifuss and D. H. Langer, *Am. J. Med.*, 1988, **84**, 34–41.

55 A. Folorunso, S. Akintelu, A. K. Oyebamiji, S. Ajayi, B. Abiola, I. Abdusalam and A. Morakinyo, *J. Nanostruct. Chem.*, 2019, **9**, 111–117.

56 K. Parveen, V. Banse and L. Ledwani, *AIP Conf. Proc.*, 2016, **1724**, 020048, DOI: 10.1063/1.4945168.

57 Y. Y. Foo, V. Periasamy, L. V. Kiew, G. G. Kumar and S. N. A. Malek, *Nanomaterials*, 2017, **7**, 123.

58 W. S. Cho, M. Cho, J. Jeong, M. Choi, H. Y. Cho and B. S. Han, *Toxicol. Appl. Pharmacol.*, 2009, **236**, 16–24.

59 E. A. E. A. El-Drieny, N. I. Sarhan, N. A. Bayomya, S. A. E. Elsherbeni, R. Momtaz and H. E. D. Mohamed, *J. Microsc. Ultrastruct.*, 2015, **3**, 181–190.

60 B. Yahyaei, M. Nouri, S. Bakherad, M. Hassani and P. Pourali, *Amb. Express*, 2019, **9**, 38.

61 T. Singh, A. Jayaprakash, M. Alsuwaidi and A. A. Madhavan, *Mater. Today: Proc.*, 2021, **42**, 1166–1169.

62 J. Gupta, A. Gupta and A. K. Gupta, *J. Chemtracks*, 2014, **16**(1), 285–288.